

Nonlinear Integration of Sensory Responses in the Rat Barrel Cortex: An Intracellular Study *In Vivo*

Michael J. Higley and Diego Contreras

Department of Neuroscience, University of Pennsylvania School of Medicine, Philadelphia, Pennsylvania 19106

To study integration of converging sensory inputs on single cortical neurons, we performed intracellular recordings *in vivo* in the barrel cortex of the barbiturate-anesthetized rat. We deflected the principal whisker (PW) for each cell either alone or preceded (at 20, 50, and 100 msec) by the deflection of a small number of remote whiskers (RWs) far from the PW. The synaptic responses to both the PW and the RW were similar qualitatively and consisted of excitation followed by inhibition that comprised an early and a late component. The RW response was of smaller amplitude and more often subthreshold for action potential generation. The main effect of the RW deflection was a suppression of the subsequent response to the PW that was most pronounced at the 20 msec interval and decreased progressively at the 50 and 100 msec intervals. Suppression of the spike output of the cell was not caused by hyperpolarization (subtractive inhibition) but by a reduction in the EPSP amplitude (divisive inhibition), resulting in a highly sublinear summation of the two responses. The small decrease in input resistance caused by the RW responses is not consistent with synaptic shunting as the main cause of the reduction of the EPSP amplitude. Instead, our results suggest that suppression results from a decrease in the amount of synaptic input triggered by the PW, particularly the early excitation. We suggest that this process involves a reduction in reverberant granular cell excitation that is induced by PW deflection.

Key words: vibrissa (whisker); corticocortical; thalamocortical; suppression; sublinear; disfacilitation

Introduction

Neocortical neurons *in vivo* receive a constant barrage of spontaneous and sensory-driven synaptic inputs from multiple sources, including thalamocortical and corticocortical pathways. Input integration is strongly affected by the intrinsic electrophysiological properties of single cells (Llinas, 1988) as well as the characteristics of the local neuronal circuit, such as recurrent excitation and feedforward and feedback inhibition. Here, we used the whisker-barrel system of the rat as an experimental model to study integration of inputs arising from different sources and targeting different elements of the local network.

The neural representation of the 30 to 35 vibrissae in the mystacial pad is organized into anatomically segregated cytochrome oxidase-rich aggregates of neurons called barrels in cortical layer 4 (Woolsey and Van der Loos, 1970; Welker and Woolsey, 1974). Barrel cells are excited most strongly by deflection of the corresponding vibrissa, termed the principal whisker (PW) (Welker, 1976; Simons, 1978). Recordings in supragranular and infragranular cortical layers, however, have revealed that these cells possess receptive fields much larger than those of the layer 4 neurons in the same barrel column, often spanning several vibrissae beyond the PW (Simons, 1978; Chapin, 1986; Armstrong-

James and Fox, 1987; Kleinfeld and Delaney, 1996; Moore and Nelson, 1998).

Anatomical studies have demonstrated that there is limited divergence of thalamocortical projections to layer 4 or intracolumnar projections of layer 4 cells to other lamina (Jensen and Killackey, 1987; Hoeflinger et al., 1995; Arnold et al., 2001; Feldmeyer et al., 2002). However, Gottlieb and Keller (1997) found that supragranular and infragranular neurons may extend axon collaterals to surrounding columns up to 2 mm distant, and lesions of individual barrels reduce the response of adjacent supragranular cells to deflection of the lesion-associated whisker (Goldreich et al., 1999). Thus, individual cortical neurons may be conceptualized as receiving two separate input “channels”: (1) direct input originating from thalamocortical projections to the corresponding barrel and local intracolumnar circuitry and (2) horizontal corticocortical input from more remote barrel columns.

The present study was designed to explore the integration of multiple inputs to cortical neurons in the barrel cortex. We activated a direct thalamocortical pathway by deflecting the PW and an indirect corticocortical pathway by deflecting a small number of remote whiskers (RWs) far from the PW. Previous extracellular studies have shown that deflection of one whisker can suppress the spikes in response to subsequent deflection of an adjacent whisker (Simons, 1985; Simons and Carvell, 1989; Brumberg et al., 1996, 1999; Shimegi et al., 1999) and that this suppression is greatest for intervals of 10–20 msec.

We found that RW deflection alone does not cause strong hyperpolarizing or shunting inhibition. However, when RW deflection preceded PW deflection by 20 msec, the summation of

Received July 16, 2003; revised Aug. 21, 2003; accepted Sept. 6, 2003.

This work was sponsored by the Human Frontier Science Program Organization. We thank Jessica A. Cardin, Gene Civillico, Larry Palmer, Noah Roy, and Bryan Wilent for helpful comments in preparation of this manuscript.

Correspondence should be addressed to Diego Contreras, Department of Neuroscience, University of Pennsylvania School of Medicine, 215 Stemmler Hall, Philadelphia, PA 19106-6074. E-mail: diegoc@mail.med.upenn.edu.

Copyright © 2003 Society for Neuroscience 0270-6474/03/2310190-11\$15.00/0

responses was highly sublinear, primarily because of a divisive reduction of the PW response. Our results suggest that such nonlinearity was caused by reduction of synaptic input, or disfacilitation. This phenomenon was seen most strongly for the early components of excitation, leading to suppression of the response to the PW and reduction of the spike output of the cell.

Materials and Methods

Surgery and preparation. Experiments were conducted in accordance with the ethical guidelines of the National Institutes of Health and with the approval of the Institutional Animal Care and Use Committee of the University of Pennsylvania. Adult male Sprague Dawley rats (350–450 gm) were anesthetized with pentobarbital (50 mg/kg, i.p.). Buprenorphine (0.03 mg/kg, s.c.) was administered to provide additional analgesia. Animals were paralyzed with gallamine triethiodide and artificially ventilated. End-tidal CO₂ (3.5–3.7%) and heart rate were continuously monitored. Body temperature was maintained at 37°C via servo-controlled heating blanket and rectal thermometer (Harvard Apparatus, Holliston, MA). The depth of anesthesia was maintained by supplemental doses of the same anesthetic to keep a constant high-amplitude, low-frequency electroencephalogram (EEG) as recorded from a bipolar electrode lowered into the cortex.

For cortical intracellular recordings, the animal was placed in a stereotaxic apparatus, and a craniotomy was made to expose the surface of the barrel cortex (1.0–3.0 mm posterior to bregma, 4.0–7.0 mm lateral to the midline). The dura was resected over the recording area, and mineral oil was applied to prevent desiccation. The stability of recordings was improved by drainage of the cisterna magna, hip suspension, and filling of the holes made for recording with a solution of 4% agar.

Electrophysiological recordings. Intracellular recordings were performed with glass micropipettes pulled on a P-97 Brown-Flaming puller (Sutter Instruments, Novato, CA). Pipettes were filled with 3 M potassium acetate and had DC resistances of 80–90 MΩ. The intracellular recording pipette was lowered into the brain ~1 mm away from the EEG electrode. Pipettes were oriented normal to the cortical surface, and the vertical depth was read on the scale of the micromanipulator. A high-impedance amplifier (bandpass of 0–5 kHz) with active bridge circuitry was used to record and inject current into the cells. Data were digitized at 10 kHz using a Power 1401 data acquisition system and Spike2 software (Cambridge Electronic Design, Cambridge, UK) and saved to disk for offline analysis.

Whisker stimulation. Individual whiskers were mechanically driven using an 8 Ω 3.5 inch speaker to which was attached a small needle. Before recording, whiskers were trimmed to a length of ~10 mm. After obtaining a stable intracellular recording, a whisker was hooked through the eye of the needle and square 100 msec electrical pulses were applied to the speaker, resulting in a step-and-hold deflection of the whisker of ~750 μm. For all experiments described here, the whisker was deflected in a ventral direction. Stimuli were applied to several whiskers in succession until the principal whisker, defined as the whisker that evoked the largest depolarizing response from resting membrane potential (see Fig. 2), was determined. Stimuli were delivered at 0.5 Hz or less to prevent steady-state adaptation of whisker-evoked responses.

To stimulate remote whiskers, a picospritzer was used to direct a small puff of air (60 msec, 0.1 pounds) to a small number of additional whiskers located at least three rows away from the PW. Visual inspection of the whisker movement caused by the air puff was used to ensure that whiskers closer to the PW were never deflected. The RW stimulus never visibly moved the PW and was also directed in the ventral direction. For the experiments described here, the puff to the RW was delivered alone or before deflection of the PW by 100, 50, or 20 msec. In some cases, whisker deflection protocols were coupled to square current pulses injected through the micropipette to record synaptic responses at different membrane potentials (V_m values). The amount of current injected was adjusted for each cell depending on the input resistance and firing rate of the cell at depolarized potentials.

Data analysis. All data analysis was done offline. Routines for averaging sensory responses and spike removal were written in Matlab (Math-

Works, Natick, MA) and Igor Pro (WaveMetrics, Lake Oswego, OR). Spikes were removed by detecting the spike threshold at the base of the action potential and extrapolating the V_m values from the start to the end of the spike. Next, a three-point running average was applied to smooth the trace. For all cells, whisker-evoked postsynaptic potential amplitudes were measured from the resting baseline V_m to the peak of the response. Baseline V_m was calculated as the mean V_m for the 500 msec before whisker deflection. All statistical measures were calculated using Prism software (GraphPad Software, San Diego, CA).

Results

We recorded intracellularly from 57 neurons in the barrel cortex of 34 barbiturate-anesthetized rats. Of these cells, 32 met our criteria for analysis (i.e., a stable resting V_m of at least –60 mV throughout the whisker stimulation protocol and overshooting action potentials). The range of resting V_m for all cells was –60 to –80 mV, and the input resistance (R_{in}) at rest was 23.7 ± 7.7 MΩ (mean \pm SD). The mean spontaneous firing rate for all cells was 2.0 ± 1.3 Hz (mean \pm SD).

Intrinsic properties of cortical neurons

Cells were classified electrophysiologically according to their firing pattern in response to depolarizing square current pulses (Fig. 1) as regular spiking (RS) ($n = 24$) or intrinsically bursting (IB) ($n = 8$). This classification followed criteria established *in vitro* (Connors et al., 1982; McCormick et al., 1985) and *in vivo* (Nunez et al., 1993). RS cells (Fig. 1A) typically fired accommodating trains of single action potentials with frequencies proportional to the pulse amplitude. RS spikes had durations of ~1 msec and small afterhyperpolarizations (Fig. 1A, inset). IB cells (Fig. 1B) typically fired repetitive bursts of two to six action potentials (spike duration, 1.0–1.5 msec) with pronounced inactivation and riding on a slower depolarizing envelope (Fig. 1B, inset). The intraburst frequency was ~300 Hz, and the interburst frequency was ~10 Hz. IB cells fired single action potentials when stimulated with lower amplitude pulses (Fig. 1B). Hyperpolarizing pulses revealed an absence of inward rectification. Of the cells recorded in this study, the majority were located at depths corresponding to infragranular layers. The remaining cells were found at depths corresponding to deep supragranular and granular layers. RS cells were located throughout the depth of the cortex, whereas IB cells were found only in infragranular layers (Fig. 1C).

Characterization of sensory responses

To study integration of synaptic inputs from different sources in barrel cortex, we deflected the PW for 32 cells with a step and hold stimulus lasting 100 msec. Whisker deflection was in a fixed ventral direction from the resting position. The PW for each cell was functionally defined as the whisker, the deflection of which caused the largest amplitude depolarization. This was associated frequently with a suprathreshold response (Fig. 2). Given the extensive subthreshold receptive fields of barrel cortex neurons (Moore and Nelson, 1998; Zhu and Connors, 1999; Brecht and Sakmann, 2002b), we tested a minimum of six whiskers before determining the PW for each cell. We also stimulated a small number (3 ± 1) of RWs at least three (4 ± 1) rows away with an air puff (60 msec) from above producing a ventral movement from the resting position. For the RS cell (depth, 1374 μm) in Figure 2A (superimposed traces are two examples of individual responses), deflection of the C2 whisker at rest (–74 mV) caused the largest EPSP (7.5 mV, spikes removed) (see Materials and Methods) as well as the largest spike output [0.5 spikes per deflection (inset histograms), accumulated over 20 deflections] and

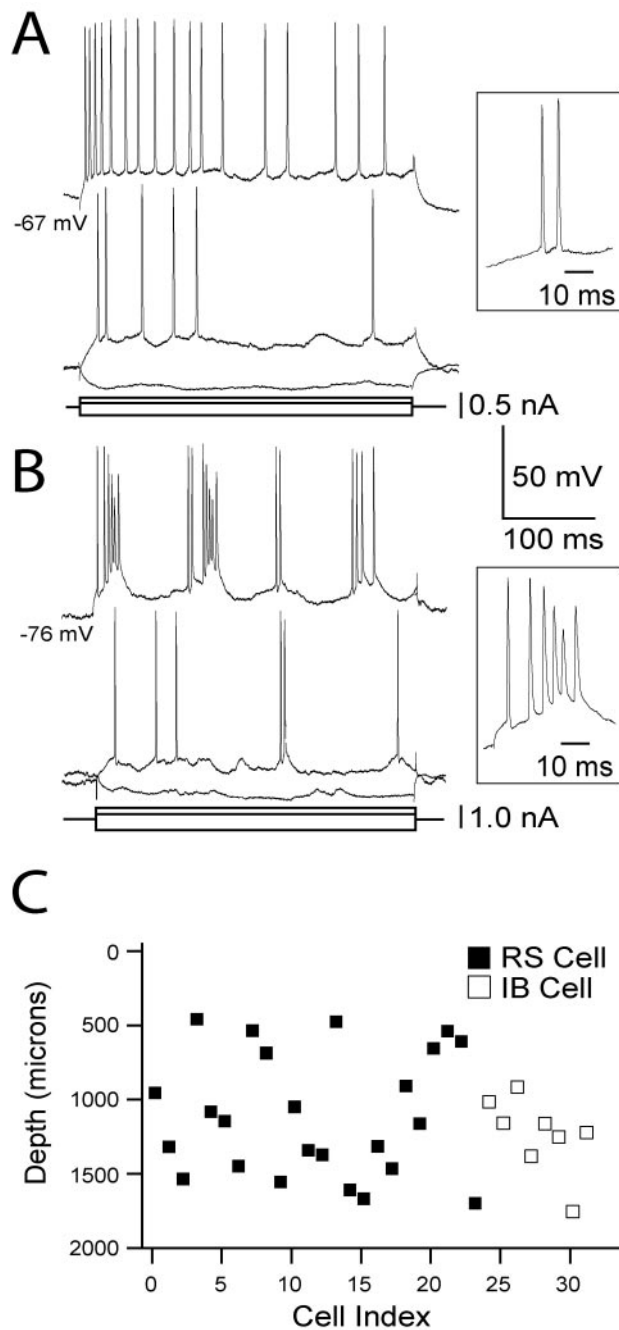


Figure 1. Intrinsic firing patterns of recorded barrel cortex neurons. *A*, Example of an RS cell that responded with an accommodating train of action potentials (from 250 to 60 Hz) to a 0.44 nA, 350 msec current pulse. A lower amplitude pulse (0.24 nA) generated a spike train of lower frequency (50 Hz) and shorter duration. A hyperpolarizing pulse (-0.44 nA) was used to determine the R_{in} at rest (34.1 M Ω). RS action potentials lasted ~ 1 msec and showed small but clear afterhyperpolarizations (inset). In this and all figures, membrane potential is indicated. *B*, An example of an IB cell that generated repetitive (10–12 Hz) bursts (inset) of two to five spikes at 300 Hz in response to a 0.94 nA, 350 msec depolarizing current pulse. A lower amplitude current pulse (0.50 nA) generated single spikes mostly, although not a regular train. *C*, Scatter plot of recorded cell types versus cortical depth. Depth indicated is relative to the brain surface as measured on the micromanipulator. RS cells ($n = 24$) were found at all depths, whereas IB cells ($n = 8$) were only found in deeper layers.

had the shortest latency to onset (7.3 msec). The next largest response was from whisker C1 (6.2 mV, 0.3 spikes per deflection, 7.9 msec latency). The other three whiskers tested caused smaller amplitude EPSPs at even longer latencies (B2, 6.1 mV, 0.4 spikes

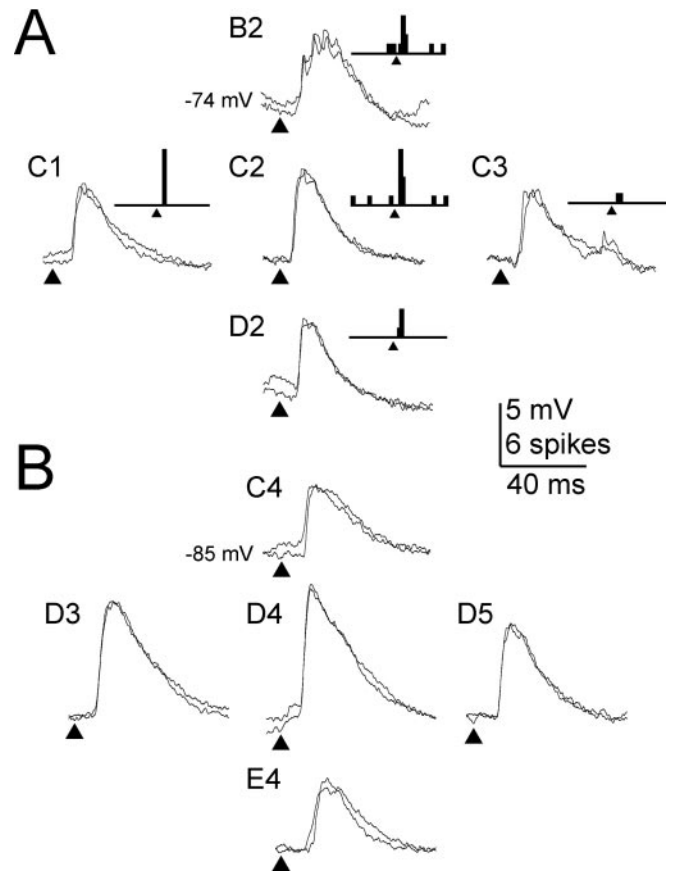


Figure 2. Receptive field mapping of barrel cortex neurons. *A*, Synaptic responses and spike histograms in response to deflection of five whiskers obtained at rest (-74 mV) from an RS cell at a depth of 1374 μm . Two individual superimposed traces are shown. The whisker that caused the largest EPSP (7.5 mV) and the most spikes (0.5 spikes per deflection) was C2 and therefore deemed the PW. *B*, Synaptic responses to five different whiskers during DC hyperpolarization (-85 mV) from an RS cell at 1096 μm depth. Hyperpolarization enhanced the difference between whiskers and showed that D4 was the PW for this cell.

per deflection, 11.6 msec; D2, 5.6 mV, 0.2 spikes per deflection, 8.1 msec; C3, 5.3 mV, 0.1 spikes per deflection, 8.1 msec). Interestingly, although three of the adjacent whiskers (C1, C3, and D2) had latencies < 1 msec longer than the PW (C2), the latency to B2 was > 4 msec longer than the PW, showing a strong asymmetry in the organization of the receptive field of this neuron. For some cells, the amplitude of depolarization from rest was small and very similar for different whiskers. In those cases, the receptive field was remapped under DC hyperpolarization to increase the amplitude of the synaptic responses. For the RS cell (depth, 1096 μm) in Figure 2*B* (DC, -0.36 nA; V_m , -85 mV), the PW-evoked response (D4, 10.7 mV, 8.1 msec latency) was only 1 mV larger than the D3 response (latency, 9.1 msec). At this V_m , the depolarizing response most likely includes a combination of excitation and reversed inhibition. However, previous studies have shown that the PW also evokes the largest inhibition of all whiskers (Simons, 1985), consistent with our definition of the PW even under hyperpolarization. The other three whiskers caused depolarizations of smaller amplitude and longer latency (C4, 5.4 mV, 10.7 msec; D5, 7.6 mV, 11.4 msec; E4, 5.9 mV, 12.2 msec). Because this cell was hyperpolarized, none of the responses reached threshold for firing action potentials.

To elucidate the nature of the synaptic responses, we deflected the PW while holding the cell at different V_m values by means of current injection through the micropipette (Fig. 3). Measuring

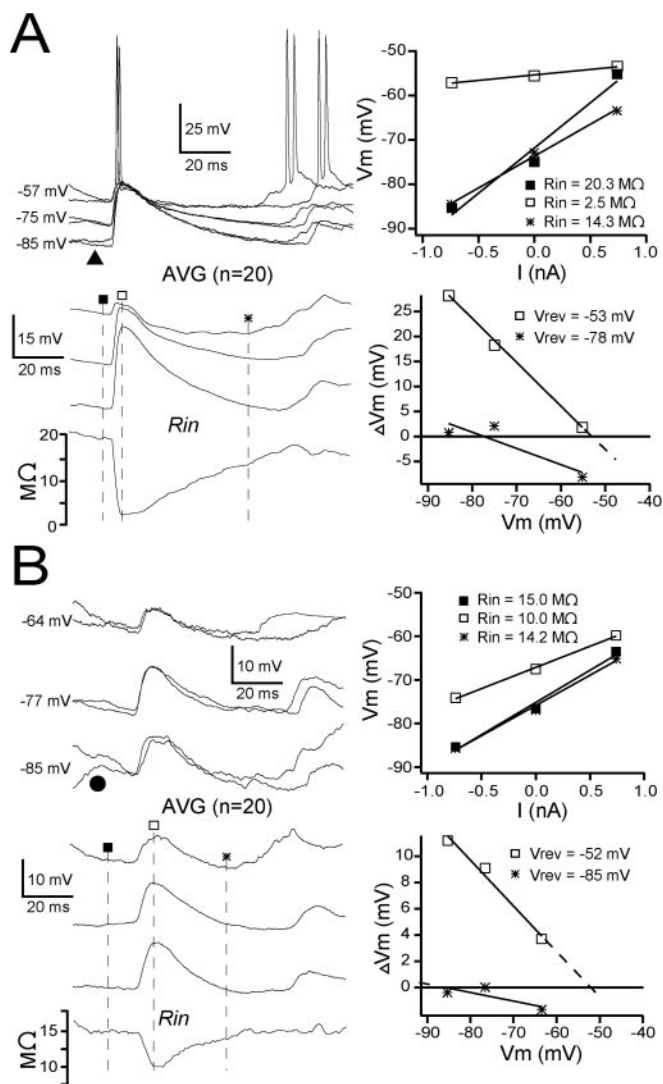


Figure 3. Measurement of R_{in} and V_{rev} of whisker-evoked responses in barrel cortex neurons. *A*, An RS cell at a depth of 536 μm responded to step-and-hold whisker deflections of 100 msec duration with an EPSP–IPSP sequence. V_m at rest (-75 mV) was displaced to depolarized (-57 mV) and hyperpolarized (-85 mV) levels by means of current injection. Top group of traces shows two individual superimposed responses at each V_m , and triangle indicates time of PW deflection. Bottom traces show the average (AVG) of 20 whisker deflections at each V_m . The trace below AVG is the R_{in} (axis at left) calculated for each time point from the three AVG traces. Measurements to construct the plots shown at right were made at the baseline (filled squares), the peak of EPSP at rest (open squares), and the peak of the long IPSP (stars). The top plot is the V – I plot. Lines are the best linear fit to each set of data points, and R_{in} (values are indicated) is the slope of the line. The bottom plot is the value of the change in V_m from baseline versus the value of baseline (ΔV_m vs V_m). Lines are the best linear fit, and the V_{rev} (values are indicated) is the V_m value at the x -intercept. *B*, The same plots as in *A* for response to RW; filled circle indicates time of RW deflection.

synaptic responses at different V_m values allowed us to estimate the apparent reversal potential (V_{rev}) and R_{in} . Figure 3*A* (top traces) shows responses to deflection of the PW (filled triangle indicates onset of deflection) from an RS cell (536 μm depth). Two superimposed individual responses are shown for each of three V_m values: rest (-75 mV), a depolarized level (-57 mV, 0.37 nA), and a hyperpolarized level (-85 mV, -0.37 nA). The average of all responses ($n = 20$) for each V_m is shown below with spikes removed (Fig. 3*A*, AVG). The response to the PW was characterized by an EPSP with 6.6 msec latency followed by a long-lasting IPSP. The long IPSP was reversed completely at rest

and was only visible by its change in polarity at the depolarized V_m . For this cell, the response to PW deflection was suprathreshold for all holding V_m values tested.

The cell also demonstrated a second depolarization ~ 90 msec after the PW deflection that was suprathreshold in some instances. This potential reflects a well characterized rebound effect in the local cortical network (Creutzfeldt et al., 1966; Contreras and Steriade, 1995) and was observed in many cells regardless of depth or electrophysiological cell type. However, because the present work deals with synaptic events that occur well before the onset of this rebound, the subject will not be considered here.

To estimate R_{in} , we plotted the value of V_m against injected current (Fig. 3, V – I plots) at three different time points: baseline before stimulation (filled squares), the peak of the depolarization at rest (open squares), and an arbitrary point near the peak of the long IPSP (stars). The value of R_{in} was defined as the slope of the least-squares best-fit linear function for each set of data points in the V – I plot (Fig. 3*A*, top). From a value at rest of 20.3 $M\Omega$, R_{in} dropped to only 2.5 $M\Omega$ during the peak of the depolarization and was 14.3 $M\Omega$ near the peak of the long IPSP. To determine the time course of the changes in R_{in} during the synaptic responses, we calculated R_{in} as a continuous function of time using the method described above applied to every data point in the response (R_{in} trace in AVG). The minimum R_{in} (2.5 $M\Omega$) was reached during the peak of the depolarization at rest and then returned slowly to resting values with a time course similar to that of the long IPSP.

To estimate V_{rev} , we plotted the change in V_m from baseline (Fig. 3, ΔV_m) at the same selected time points against the value of the baseline V_m . V_{rev} was defined as the value of V_m at the x -intercept of the best-fit linear function for each set of data points (Fig. 3*A*, bottom plot). The V_{rev} at the point of minimum R_{in} (open squares) was -53 mV. This value, together with the pronounced drop in R_{in} , is suggestive of an overlapping glutamatergic EPSP and GABA_A chloride-mediated IPSP. Indeed, the average trace at depolarized V_m suggests that the actual EPSP is cut short by an IPSP that coincides with the R_{in} minimum. The V_{rev} during the long IPSP was -78 mV, suggestive of a contribution from an underlying potassium current also supported by the much smaller drop in R_{in} .

These measurements were also used to characterize the response to RW deflection (Fig. 3*B*, filled circle) in the same cell. The responses showed longer latencies (16.0 msec to EPSP onset), and the individual components were of smaller amplitude (10 mV EPSP at rest compared with 13.3 mV for the PW) and subthreshold generally. The value of R_{in} was 10 $M\Omega$ at peak depolarization (open squares) and 14.2 $M\Omega$ near the peak of the long IPSP (stars). V_{rev} at the same time points was -52 and -85 mV, respectively. These values were compatible with a sequence of synaptic events similar to the PW response: an initial short EPSP followed by a fast chloride-based IPSP and a slow potassium-based IPSP.

The quantification of the synaptic responses for the whole population ($n = 32$) is shown in Figure 4. Overall, none of the measurements of synaptic responses showed a clear systematic variation with cortical depth (data not shown). The amplitude of the peak of the EPSP was measured from resting V_m (Fig. 4*A*). EPSP amplitudes in response to PW deflection ranged from 3.2 to 17.7 mV, with an average of 8.0 ± 4.3 mV (filled circle). In response to RW deflection, EPSP amplitudes ranged from 0 to 13.3 mV, with an average of 4.3 ± 3.9 mV (open circle; Student's t test; $p < 0.001$). In 15 of 32 cells, the PW response was suprathreshold for action potential generation, usually generating under one

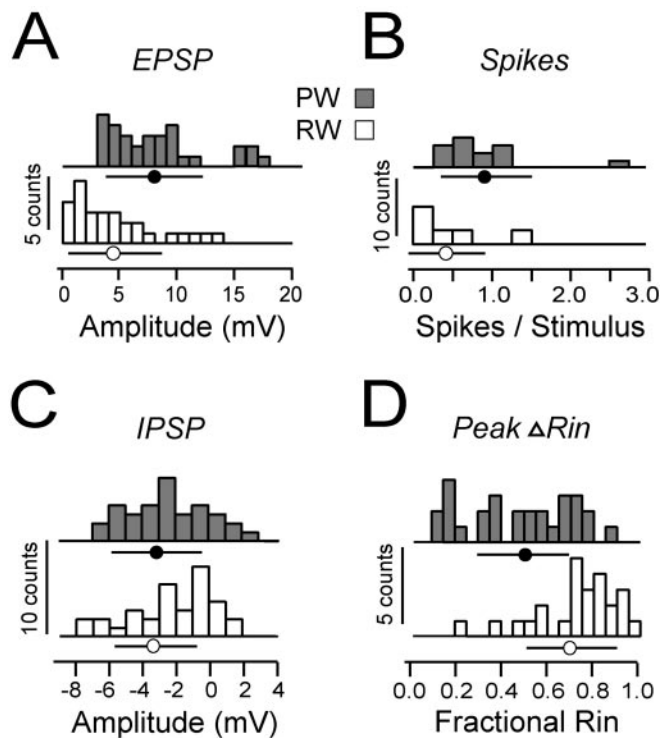


Figure 4. Summary of the response measurements from all cells ($n = 32$). The distribution of values is summarized by the histograms and by the mean \pm SD, represented by the filled (PW) and open (RW) circles below each histogram. Measurements were made from the averaged responses to 20–30 deflections. *A*, EPSP amplitude was measured at the peak (bin size, 1 mV). Means for the whole population were 8.0 ± 4.3 mV (PW deflection alone) and 4.3 ± 3.9 mV (RW deflection alone) (Student's t test; $p < 0.001$). *B*, Spike output was measured as spikes per whisker deflection (bin size, 0.25 spikes per stimulus). Subthreshold cells are represented with a value of 0. The mean values of all suprathreshold cells for PW deflection was 0.8 ± 0.6 spikes per stimulus, and the mean for RW deflection was 0.4 ± 0.5 spikes per stimulus ($p < 0.01$). *C*, Amplitude of the long IPSP was measured from rest at the time of peak hyperpolarization (bin size, 1 mV). There was no significant difference between PW response (-3.2 ± 2.7 mV) and RW response (-3.4 ± 2.5 mV). *D*, Peak change in R_{in} was measured as the ratio of the minimum of the continuous plot of R_{in} (as in Fig. 3) to the baseline R_{in} (bin size, 0.05). The mean for PW deflection was 0.50 ± 0.20 , and the mean for RW deflection was 0.70 ± 0.20 ($p < 0.001$).

spike per deflection (0.8 ± 0.6 spikes per deflection, filled circle) (Fig. 4*B*). RW stimulation was suprathreshold in 7 of 32 cells (0.4 ± 0.5 spikes per deflection, open circle; $p < 0.01$)

The amplitude of the long IPSP was measured from rest at the time of the peak hyperpolarization as determined from a depolarized V_m (Fig. 4*C*). Thus, positive values reflect IPSPs that were reversed at resting V_m . The amplitudes of the long IPSP showed no significant difference between responses to PW (-3.2 ± 2.7 mV, filled circle) and RW (-3.4 ± 2.5 mV, open circle).

Finally, we calculated the peak change in apparent R_{in} caused by both PW and RW deflection (Fig. 4*D*). Fractional R_{in} was expressed as a ratio of the R_{in} at the peak to the R_{in} at rest (thus, fractional $R_{in} = 1$ for no change). Deflection of the PW and RW resulted in an average fractional R_{in} of 0.50 ± 0.20 (filled circle) and 0.70 ± 0.20 (open circle), respectively ($p < 0.001$). In summary, the typical response pattern to deflection of either PW or RW was an excitation followed by a longer latency inhibition. Although there was variability in the data, the RW evoked less excitation generally and caused a smaller drop in the R_{in} of the cell compared with the PW-evoked response.

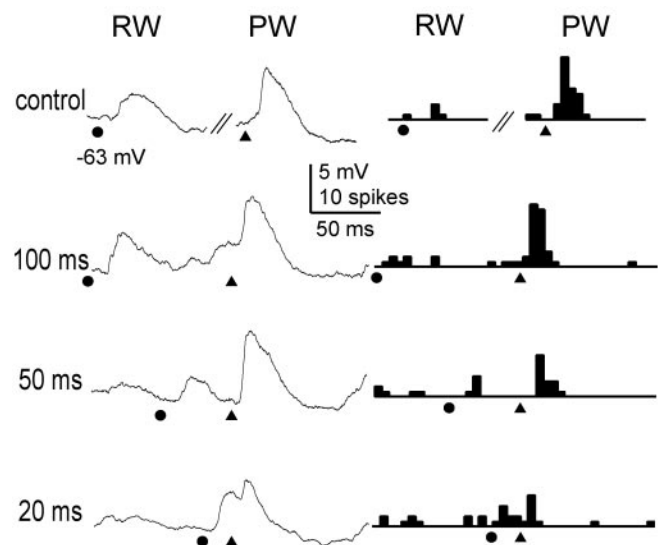


Figure 5. Interaction between PW and RW at different intervals. Example of one RS cell at $688 \mu\text{m}$ depth. PW was D2. Left traces are average V_m ($n = 20$ deflections) at rest (-63 mV), and right traces are the cumulative spike histograms. Control shows the responses to both PW and RW deflection alone. Times at left indicate interval by which RW deflection (filled circle) preceded PW deflection (filled triangle). EPSP amplitude and spike output to PW deflection alone (7 mV, 1.4 spikes per deflection) were suppressed at the 20 msec interval (4.6 mV, 0.5 spikes per deflection). Spike output was also reduced at the 50 msec interval, despite minimal change in EPSP amplitude. No change was observed at the 100 msec interval.

Integration of sensory responses

To study the integration of synaptic responses caused by the two stimuli, the RW was deflected before the PW at three intervals: 100, 50, and 20 msec, similar to previous extracellular studies (Simons, 1985; Simons and Carvell, 1989). A representative example from an RS cell ($688 \mu\text{m}$ depth) is shown in Figure 5. The average ($n = 20$) response to deflection of either the RW or the PW at rest (-63 mV, control) comprised an EPSP with amplitude of 3.3 and 5.8 mV, respectively, followed by a longer IPSP. When the RW preceded the PW by 100 or 50 msec, the EPSPs were clearly separated in time, and little change was observed in the average EPSP to the PW deflection. When the interval was 20 msec, the response to the PW was riding on the decaying phase of the RW response. Although the calculated linear sum of the two responses would have been ~ 9.1 mV ($3.3 + 5.8$ mV), the actual summed response was only 4.6 mV, a value even lower than the response to the PW alone. As a result of this suppression, the spike output decreased from a control response of 1.4 spikes per deflection to 0.5 spikes per deflection for the 20 msec RW–PW interval. For this cell, the spike output for the 50 msec interval was also slightly reduced, despite the fact that the average EPSP was not different from control values. No change was observed for the 100 msec interval.

We quantified the effect of RW deflection on the spike output to the PW for all cells with suprathreshold responses (Fig. 6*A*, Spikes). We expressed this effect as a ratio of the spike counts in the first 25 msec after PW deflection when preceded by the RW to those in the first 25 msec after PW deflection alone (response ratio). Thus, a value of 1 indicates no effect of preceding RW deflection, values > 1 indicate facilitation, and values between 0 and 1 indicate suppression. At the 20 msec interval, most cells had response ratios (14 of 16) below 1 (dotted line), and four cells showed complete suppression of their responses. Only two cells showed facilitation. At the 50 msec interval, 11 cells showed suppression, and five cells showed facilitation. At the 100 msec inter-

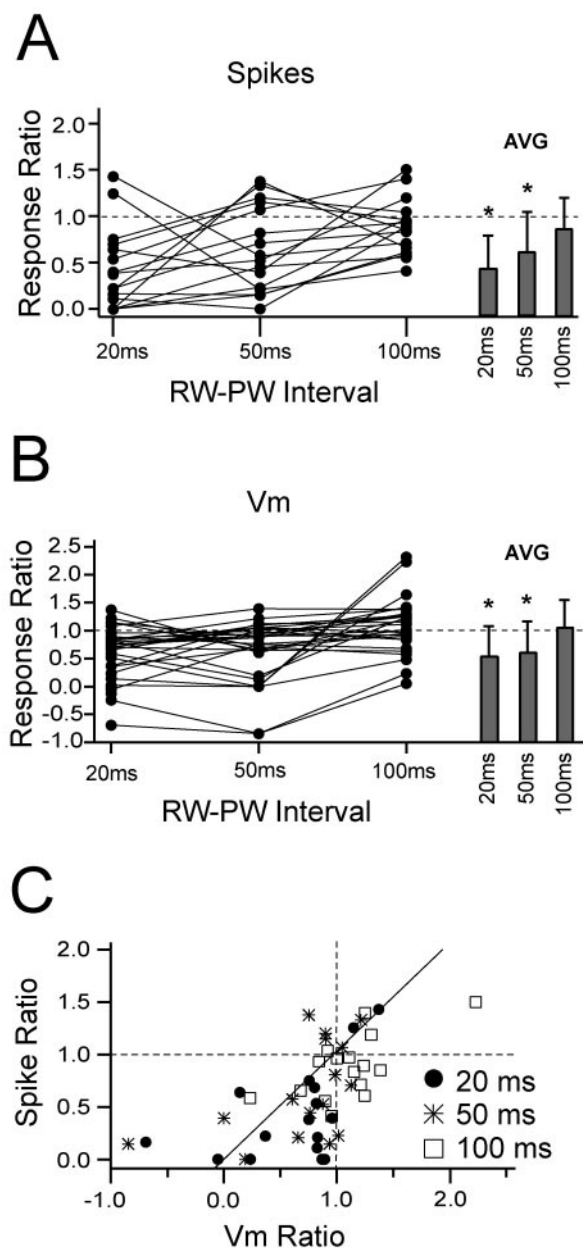


Figure 6. Summary plot of the suppression and/or facilitation of V_m and spikes for the whole population. Suppression and/or facilitation was calculated as the ratio of the amplitude of the RW–PW response to the amplitude of the PW response (response ratio). Dots represent the value of this ratio for spike output in *A* and EPSP amplitude in *B*. Lines connect values from each cell across each of three RW–PW intervals (20, 50, and 100 msec). Bars at right represent the mean \pm SD for each interval. In *A*, average (AVG) values differed significantly from 1 for the 20 msec (response ratio, 0.42 ± 0.44 ; $p < 0.001$) and 50 msec (response ratio, 0.64 ± 0.46 ; $p < 0.01$) intervals (marked with asterisks) but not the 100 msec (response ratio, 0.88 ± 0.30) interval. For the same intervals, the means for V_m in *B* were 0.58 ± 0.47 ($p < 0.001$), 0.64 ± 0.56 ($p < 0.01$), and 1.08 ± 0.50 (NS), respectively. *C*, Values of response ratio from *A* and *B* are plotted against each other. Most points are below the main diagonal (solid line), indicating that changes in V_m resulted in larger changes in spike output.

val, response ratios were distributed almost equally on both sides of the identity line, and in no instance was there a complete suppression of the output. The average values were significantly <1 for the 20 msec interval (0.42 ± 0.44 ; Student's *t* test; $p < 0.001$) and the 50 msec interval (0.64 ± 0.46 ; $p < 0.01$). The ratio for the 100 msec interval did not differ significantly from 1 (0.88 ± 0.30).

Because spike output depends presumably on the level of V_m reached by whisker-evoked EPSPs, we also quantified suppression and/or facilitation of the V_m responses. As with the spike data, the effect was expressed as a ratio of the peak amplitude of the PW-evoked EPSP measured from baseline when preceded by the RW to the peak amplitude of the EPSP evoked by the PW alone (Fig. 6*B*, V_m). Again, the response ratio equals 1 for no change in the PW amplitude. Values >1 indicate facilitation, and values <1 indicate suppression. In contrast with the spike data, the V_m can assume values below baseline, in which cases, the value of the response ratio is negative. The values obtained for V_m were consistent with the spike data. The strongest suppressive effect was at the 20 msec interval (27 of 32 cells), including five cells in which the peak V_m was hyperpolarized below baseline (response ratio <0). The peak V_m was above control (facilitation) for only five cells. V_m suppression was also observed at the 50 msec interval (20 of 28 cells), but, at the 100 msec interval, response ratios were distributed evenly on both sides of the identity line. Average values were significantly <1 for the 20 msec (0.58 ± 0.47 ; $p < 0.001$) and 50 msec (0.64 ± 0.56 ; $p < 0.001$) intervals. The response ratio for the 100 msec interval did not differ significantly from 1 (1.08 ± 0.50).

To verify whether changes in the response ratio of spike output could be accounted for by changes in the response ratio of the V_m , we plotted one set of values against the other (Fig. 6*C*). Spike ratio correlated weakly with V_m ratio (Pearson's correlation; $r^2 = 0.37$; $p < 0.001$). However, the weakness of the relationship is likely attributable in part to the fact that spike ratio cannot assume values below 0, despite negative values for V_m ratio. Importantly, most points were located below the main diagonal (solid line), indicating that, in general, suppression of V_m caused disproportionately larger suppression in spike output. Additional understanding of this relationship requires specific knowledge of how V_m is transformed into spike output for each individual cell.

Suppression or facilitation of the PW-evoked response can be achieved by the following: (1) decreasing or increasing the amplitude of the EPSP or (2) hyperpolarizing or depolarizing the baseline V_m . These two processes are equivalent to the algebraic operations of multiplication and addition, respectively, and are not mutually exclusive. In the case of suppression, the multiplication component is smaller than 1 (i.e., division) and/or the addition component is negative (i.e., subtraction). These operations have been shown to correspond to well known cellular processes (Coombs et al., 1955; Llinas et al., 1974; Holt and Koch, 1997). To estimate the contribution of each operation to the V_m response ratio, we made three measurements for each cell as shown for two example neurons in Figure 7*A*: *a*, the amplitude of the EPSP, measured from resting baseline, in response to the PW alone; *b*, the displacement from resting baseline caused by the RW alone, measured at the time of the peak of the PW response; and *c*, the amplitude of the EPSP to the PW when preceded by the RW, measured from *b*. Because the suppression was strongest and most consistent when the RW preceded the PW by 20 msec, we focused our analysis solely on that interval.

To compare across cells, both the additive and multiplicative components were expressed as ratios of the amplitude of the control EPSP, or *a*. Thus, the additive component was the fractional shift in baseline caused by the RW, or b/a , and the multiplicative component was the ratio of the PW responses, with and without the preceding RW, or c/a . The sum of the two components results in the total amount of suppression and/or facilitation, or $(b + c)/a$. This value is the response ratio, as explained for Figure 6*B*, and is equivalent to the ratio of the amplitude from

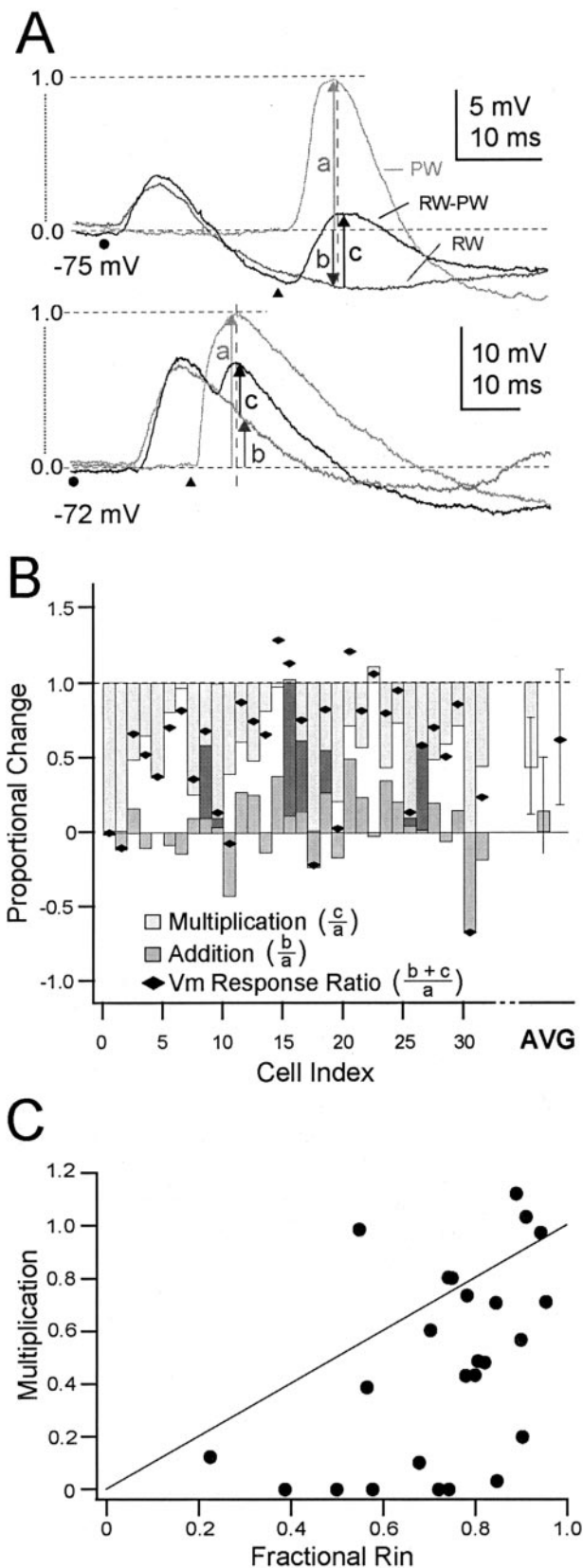


Figure 7. Contribution of additive and multiplicative processes to suppression and/or facilitation. *A*, Two examples of integration of the responses to RW (filled circle) and PW (filled triangle) deflection. Measured values were as follows: *a*, amplitude of EPSP evoked by PW alone measured at the peak from resting V_m (-75 mV); *b*, shift in baseline caused by the RW alone, measured at the time in which the peak of the PW-evoked EPSP occurs; and *c*, peak amplitude of the PW-evoked EPSP during the combined stimulus, estimated from the previously measured *b*. In both cases, RW preceded PW by

resting baseline of the RW–PW response to the amplitude of the PW alone response.

Using these calculations, for each cell, we plotted the response ratio (same data as in Fig. 6*B*, 20 msec interval) along with the proportional change contributed by the multiplicative and additive components (Fig. 7*B*). A multiplicative component was present in all cases, and the value was <1 (a divisive effect) in all but two cells. An additive component also played a role in all cases, and it was more often positive (18 cells) than negative (a subtractive effect, 13 cells). The averages from all cells (Fig. 7*B*, AVG) show that the suppression (0.58 ± 0.47) of the PW-evoked EPSP when preceded by the RW was a result mostly of a divisive operation (0.45 ± 0.34) acting against an additive (0.13 ± 0.35) component.

It is plausible that the divisive action might be caused by an RW-evoked decrease in R_{in} (i.e., shunting inhibition), with a larger reduction in EPSP amplitude corresponding to a larger decrease in R_{in} . Figure 7*C* shows the values of the multiplicative component plotted against the minimum fractional R_{in} that occurred during the response to the RW deflection alone (values from Fig. 4*D*). Both axes cover a range from 0 (in which there is a total elimination of the EPSP and a total disappearance of a measurable R_{in}) to 1 (in which the EPSP amplitude is unchanged by the preceding RW deflection and there is no change in R_{in}). If the multiplicative component (which was most often below 1 and therefore divisive) was solely attributable to shunting caused by a drop in R_{in} , one would expect an ohmic relationship between these values. However, the plotted data reveal only a weak correlation (Pearson's correlation; $r^2 = 0.24$; $p < 0.05$). Furthermore, the majority of points lie below the main diagonal, indicating that the divisive changes are larger than those predicted solely by the reduced R_{in} . These results suggest that other mechanisms contribute substantially to the divisive suppression.

To elucidate the specific synaptic components of the PW response that were modified by the preceding RW deflection, we repeated the three sets of deflections (RW, PW, and RW–PW at 20 msec) while holding the V_m at three different levels. In the example of Figure 8, the average ($n = 20$) traces (Fig. 8*A*, V_m , AVG) at rest (-71 mV) show that the synaptic response to both the PW (light gray trace) and the RW (dark gray trace) deflection consisted of excitation followed by inhibition. These synaptic responses elicited consistent spikes for the PW (1.1 spikes per deflection) but were subthreshold for the RW (Fig. 8*A*, Spikes, middle histograms). When the RW deflection preceded the PW by 20 msec (black trace), there was a suppression of the EPSP

←

20 msec (note the different calibration in each case). In top traces, the PW response rode on an RW-evoked hyperpolarization, whereas in the bottom traces, the PW response rode on a depolarization. *B*, Suppression–facilitation (filled diamonds) was measured as the amplitude from baseline of the PW-evoked EPSP when preceded by the RW ($b + c$), divided by the amplitude of the EPSP to the PW alone (a). Values below 1 indicate suppression, and values above 1 indicate facilitation. The proportional change contributed by the additive component was calculated as the shift in baseline (b) and expressed as a fraction of a (b/a). Values of addition below 0 indicate subtraction (baseline shifted downward), and values of addition above 0 indicate baseline shifted up. The proportional change contributed by the multiplicative component was calculated as the fractional change in the ΔV_m evoked by the PW (c/a). Values of multiplication below 1 indicated a divisive effect (EPSP amplitude decreased), and values above 1 indicated a multiplicative effect (EPSP amplitude increased). Response ratio is equal to the sum of the additive and multiplicative components. AVG, Average. *C*, Plot of the ratio of the multiplicative component from *B* versus the minimum fractional R_{in} that occurred during the response to RW deflection alone (from Fig. 4*D*). The changes in EPSP amplitude correlated weakly (Pearson's correlation; $r^2 = 0.24$; $p < 0.05$) with changes in R_{in} .

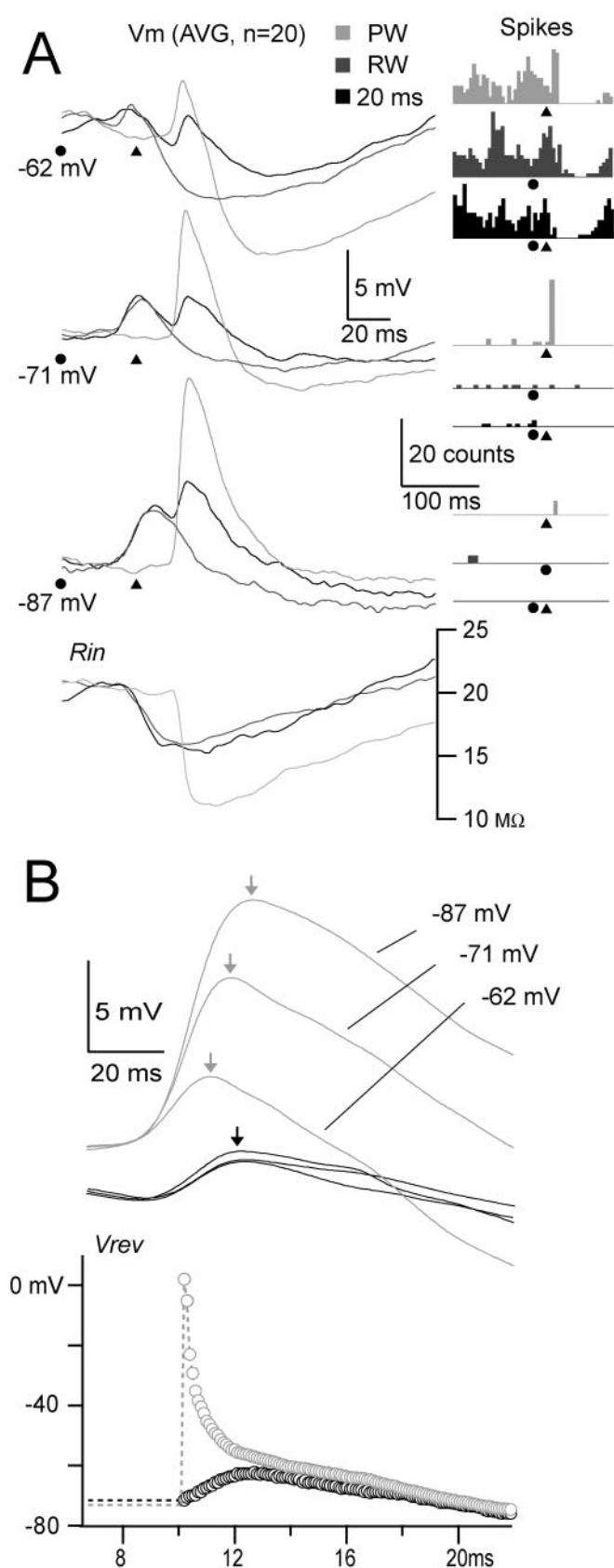


Figure 8. Suppression occurs with reduction in overall conductance and elimination of an initial fast excitatory component. *A*, Example of average (AVG) responses ($n = 20$) of an IB cell located at 1224 μm . Traces are responses to PW alone (light gray), RW alone (gray), and RW preceding PW by 20 msec (black). Spike histograms obtained from the same responses are represented at right (Spikes). The three sets of stimuli were presented under three currents

(response ratio, 0.23), and the spike output to the PW was completely abolished (response ratio, 0). In this case, the V_m suppression comprised both an additive component (-0.20) and a multiplicative component (0.43), which was reflected in the reduction of the EPSP amplitude from 9.0 to 3.9 mV. Depolarizing the cell (-62 mV, 0.67 nA) revealed a strong IPSP in response to both PW and RW, also evident in the spike histograms by the reduction in firing after the initial response and the sharp decrease in R_{in} . Under hyperpolarization (-87 mV, -0.70 nA), the response was almost entirely depolarizing because of the reversal of the IPSP, and the spike output was greatly reduced. The plot of continuous R_{in} (Fig. 8*A*, bottom traces) showed that the large drop in R_{in} associated with the response to the PW alone was virtually absent after the combined RW–PW deflection.

The effect of the preceding RW deflection was made clearer when the V_m traces were offset artificially such that the baselines immediately preceding the response to the PW were aligned (Fig. 8*B*). The offset traces for the PW alone (light gray) highlight the increase in response amplitude and a rightward shift in peak latency (light gray arrows) (from 10.8 msec at -62 mV to 12.6 msec at -87 mV) as the V_m is hyperpolarized progressively. In contrast, the traces for the RW–PW response (black) showed that hyperpolarization caused little change in the amplitude of the response and no shift in peak latency, which had a constant value of 12.3 msec (black arrow).

The shift in peak latency and the increase in amplitude of the PW-alone response were caused by the gradual reversal of the IPSP and were absent after RW deflection. These findings, together with the reduction of the drop in R_{in} (Fig. 8*A*), suggest that the RW deflection suppressed most of the synaptic input triggered by the subsequent deflection of the PW, particularly the early excitation. To support this hypothesis, we calculated continuous plots of V_{rev} for the PW alone and the RW–PW responses (Fig. 8*B*, bottom). Because the V_m traces overlap during the first few milliseconds of the response, the calculation of V_{rev} is not defined over this interval (because the slope of the ΔV_m vs V_m line is 0), and these points are shown as dashed lines in the figure. Our plot of V_{rev} values begins at the first time point that the V_m traces diverge. The synaptic response to the PW alone (light gray open circles) had an early V_{rev} of 2.1 mV at 10 msec that decreased rapidly to -58 mV at 12 msec. The V_{rev} then decreased slowly toward -80 mV near the peak of the hyperpolarization (~ 30 msec). This pattern is compatible with a response composed of an early glutamate-mediated EPSP followed by a fast GABA_A-mediated IPSP and a slower K⁺-based hyperpolarization. In contrast, when the response to the PW was preceded by deflection of the RW (black open circles), the initial excitatory component was completely absent, and the values of V_{rev} reached slowly -62 mV at ~ 12 msec, subsequently assuming very similar values as the PW alone response and reaching -80 mV at the peak of the hyperpolarization. This finding, coupled with the reduced drop in R_{in} (Fig. 8*A*), suggests that the early EPSP was suppressed greatly but the following IPSP was still present, albeit reduced in magnitude.

In summary, the observed suppression is achieved mostly by a reduction of the EPSP amplitude, not by hyperpolarization.

←

levels (indicated by V_m) to estimate R_{in} (bottom traces) and V_{rev} (bottom traces in *B*). *B*, Same average responses to the PW deflection alone (light gray) and RW–PW deflection (black) as in *A*, offset to the same baseline V_m for comparing timing of the peak of the EPSP (dashed line). Bottom traces are the calculated V_{rev} (axis at left) showing suppression during the response to combined stimulus, of the early component.

However, this reduction is not because of direct shunting inhibition caused by the preceding RW deflection. Instead, our findings indicate that suppression of the PW-evoked response occurs via removal of synaptic inputs or disfacilitation. In light of the fact that the time course of both suppression and whisker-evoked inhibition are similar (strongest between 10 and 20 msec and dissipating beyond 100 msec), we suggest this disfacilitation is mediated by local inhibition within layer 4, leading to suppression of the cortical column.

Discussion

Neurons in the barrel cortex receive input from their PW via a direct pathway leading from the corresponding thalamic barreloid to the appropriate barrel in cortical layer 4 (Land et al., 1995; Goldreich et al., 1999; Arnold et al., 2001; Bruno and Simons, 2002; Swadlow et al., 2002; Swadlow, 2003). From layer 4, PW-specific signals are relayed to supragranular and infragranular cells within the same column (Agmon and Connors, 1991; Armstrong-James et al., 1992; Petersen and Sakmann, 2001). However, there is evidence that the receptive fields of nongranular cells are larger than those of their respective layer 4 neurons and arise through indirect horizontal corticocortical connections from surrounding columns (Simons, 1978; Chapin, 1986; Armstrong-James and Fox, 1987; Bernardo et al., 1990; Kleinfeld and Delaney, 1996; Gottlieb and Keller, 1997; Goldreich et al., 1999; Shimegi et al., 1999). We attempted to activate both of these input channels by deflecting the PW and a small number of whiskers far from the PW. Intracellular and extracellular studies of barreloid physiology have suggested that thalamic receptive fields do not extend more than two whiskers beyond the PW (Armstrong-James and Callahan, 1991; Brecht and Sakmann, 2002a). Therefore, in the present study, all RWs were located at least three rows away from the PW to activate distinctly both the direct and indirect pathways.

For all cells, we were able to identify a PW that produced the largest response. However, as in previous studies (Moore and Nelson, 1998; Zhu and Connors, 1999; Brecht and Sakmann, 2002b), we found that the receptive fields of cortical neurons extended well beyond the PW. The spike rates of our suprathreshold cells ($n = 16$ of 32) were similar to previous extracellular studies (Simons and Carvell, 1989), indicating that our intracellular recordings did not damage the cells. Similar to other studies, amplitudes of PW-evoked EPSPs ranged from 3 and 18 mV, and excitation was generally followed by biphasic inhibition lasting up to 150 msec (Carvell and Simons, 1988; Moore and Nelson, 1998; Zhu and Connors, 1999). The early inhibitory component reversed at approximately -60 mV and caused a 10–85% decrease in the R_{in} of the cell. Such large sensory-evoked increases in membrane conductance are also found in the visual system (Borg-Graham et al., 1998). A longer latency inhibitory component reversed at approximately -85 mV and occurred with a smaller conductance change. This pattern of inhibition is similar to that seen *in vitro*, in which a fast GABA_A chloride conductance is followed by a slower potassium conductance (Connors et al., 1988).

We observed a response qualitatively similar (excitation followed by inhibition) to both PW and RW deflection, differing only in the fact that the RW response was smaller in amplitude and more often subthreshold for firing action potentials. From this finding, we conclude that the cortical response to whisker deflection is shaped strongly by the local circuit and is not simply imposed by upstream activity.

To understand the cortical integration of sensory inputs, we

examined the interaction of responses to PW and RW deflection. Consistent with the pioneering extracellular studies of Simons and colleagues (Simons, 1985; Simons and Carvell, 1989), we observed that the response to deflection of the PW could be reduced if preceded by RW deflection. To quantify the reduction, we calculated a response ratio of the magnitude of the PW-evoked response with and without a preceding RW deflection. We used this same measure for both the spike output and the V_m response (Fig. 6). The spike response ratio was less than one for the majority of cells, indicating that the output of the cell to PW deflection was suppressed when preceded by RW deflection. Underlying the reduction in spike output was a corresponding suppression of the PW-evoked EPSP. The suppression was greatest at the 20 msec interval, returning to control values by 100 msec. In addition, we found that the amount of V_m suppression only correlated weakly with spike suppression. This finding is consistent with spike generation at a specific V_m threshold, whereby only small changes in V_m near threshold are necessary to abolish spike output completely.

A number of differences exist between the present study and previous descriptions of cross-whisker suppression. Our recordings were done in barbiturate-anesthetized animals that may exhibit different sensory responses than those seen in Fentanyl-sedated rats, as studied by Simons and colleagues. Additionally, previous work has focused on response suppression within layer 4 caused by deflection of a whisker adjacent immediately to the PW (Simons, 1985; Simons and Carvell, 1989). Our recordings include cells recorded in nongranular layers, and the magnitude and mechanisms of suppression may be critically dependent on laminar position, as discussed later. Furthermore, as discussed above, deflection of remote whiskers likely engages a separate thalamocortical pathway than does PW deflection. In contrast, adjacent whisker deflection is likely to activate the same population of thalamic and cortical layer 4 neurons as the PW (Simons and Carvell, 1989; Bruno and Simons, 2002), possibly leading to a mechanistically different form of suppression.

A number of possible mechanisms might underlie the suppression reported here, including the following: (1) intrathalamic inhibition of whisker responses, (2) synaptic depression of the thalamocortical input, (3) presynaptic inhibition of thalamocortical or corticocortical synapses, (4) direct postsynaptic inhibition of cortical neurons, or (5) reduction in the synaptic input to cortical cells. Simons and Carvell (1989) have demonstrated previously that thalamic barreloid neurons do not exhibit strong cross-whisker suppression, suggesting that an intrathalamic mechanism for the present findings is unlikely. Synaptic depression of thalamocortical terminals after repeated whisker deflection can occur for input frequencies as low as 2 Hz (Chung et al., 2002). However, in the present study, the two whisker inputs (PW and RW) most likely use independent thalamocortical pathways and so are not susceptible to this type of depression. Nevertheless, this mechanism may play a role in suppression caused by adjacent whisker deflection. We cannot discard or favor presynaptic inhibition of corticocortical or thalamocortical terminals, because little is known about such mechanisms.

Direct postsynaptic inhibition has been proposed as the mechanism by which deflection of whiskers immediately adjacent can suppress the response to PW deflection (Simons, 1985; Simons and Carvell, 1989; Moore et al., 1999). Postsynaptic inhibition can cause suppression via two nonmutually exclusive mechanisms (Coombs et al., 1955; Llinas et al., 1974; Holt and Koch, 1997). Shunting inhibition occurs when an increase in membrane conductance causes a divisive reduction in the ampli-

tude of synaptic responses. Hyperpolarizing inhibition occurs when negative and positive currents sum linearly to produce a net movement of the V_m away from spike threshold. Because negative synaptic currents are produced by the opening of gated channels, hyperpolarizing inhibition necessarily includes shunting to some extent. In the present study, we showed that suppression caused by deflection of whiskers far removed from the PW was not attributable to a hyperpolarization, because the RW-evoked response was depolarizing predominantly 20 msec after deflection. Instead, we found a divisive effect in all but four cells. However, the nonlinear reduction of the postsynaptic potential was not attributable to shunting inhibition caused by an RW-evoked conductance increase, because the amount of division did not correlate with the calculated change in R_{in} caused by the preceding RW deflection (Fig. 7C). It is unlikely that we underestimated the drop in R_{in} because of electrotonic attenuation of synaptic potentials located distally in the dendritic tree for two reasons. First, most of the conductance increase is a result of activation of GABAergic synapses, which are located predominantly on the soma and proximal dendritic arbor (Tamas et al., 1997). Thus, the amount of attenuation between the synapse and the recording site should be minimal. Second, the preceding RW deflection actually reduced the PW-evoked decrease in R_{in} (Fig. 8A). These findings indicate that, at least for the population of cells recorded in this study, the observed suppression is not attributable to direct inhibition of the cell by RW deflection.

Nonlinear suppression can also be caused by a reduction of those inputs that normally drive the response to the PW, or disfacilitation (Llinas, 1964; Llinas and Terzuolo, 1964). Consistent with this hypothesis, two scenarios are possible: (1) suppression of recurrent excitatory and inhibitory loops within the local supragranular and infragranular networks and (2) suppression of layer 4 spiny stellate cells. The first possibility implies that the initial portion of the response to the PW, which is suppressed by the RW (Fig. 8), is caused mainly by local recurrent excitation. However, the PW-evoked EPSP in supragranular and infragranular layers typically ends within 2–3 msec of the onset of any suprathreshold response, making it unlikely that a large component of the EPSP itself could be caused by feedback excitation. We favor the second scenario and propose that deflection of the RW results in a decreased output from spiny stellate neurons within layer 4 to the subsequent PW deflection. Although horizontal corticocortical connections appear to terminate only in nongranular layers (Gottlieb and Keller, 1997), other work has shown that intracolumnar projections from nongranular layers target interneurons specifically within layer 4 (Thomson et al., 2002) that might mediate cross-whisker suppression. A role for inhibition is suggested further by the similar time course of suppression and whisker-evoked IPSPs. However, suppression within layer 4 does not need to be based on strong inhibition, because small changes in V_m can lead to great reductions in spike output (Fig. 6). Furthermore, previous modeling studies have suggested a strong role for recurrent excitation within layer 4 in enhancing nonlinearly the response to optimal sensory stimulation (Kyriazi and Simons, 1993; Douglas et al., 1995). It is likely that even a small amount of inhibition applied to many cells within the local network may lead to a marked reduction in the output of layer 4, leading to a disproportionately greater suppression of the columnar response. Future studies will include identified recordings within layer 4 as well as in the thalamus to study this possibility further.

References

- Agmon A, Connors BW (1991) Thalamocortical responses of mouse somatosensory (barrel) cortex *in vitro*. *Neuroscience* 41:365–379.
- Armstrong-James M, Callahan CA (1991) Thalamo-cortical processing of vibrissal information in the rat. II. Spatiotemporal convergence in the thalamic ventroposterior medial nucleus (VPM) and its relevance to generation of receptive fields of S1 cortical “barrel” neurones. *J Comp Neurol* 303:211–224.
- Armstrong-James M, Fox K (1987) Spatiotemporal convergence and divergence in the rat S1 “barrel” cortex. *J Comp Neurol* 263:265–281.
- Armstrong-James M, Fox K, Das-Gupta A (1992) Flow of excitation within rat barrel cortex on striking a single vibrissa. *J Neurophysiol* 68:1345–1358.
- Arnold PB, Li CX, Waters RS (2001) Thalamocortical arbors extend beyond single cortical barrels: an *in vivo* intracellular tracing study in rat. *Exp Brain Res* 136:152–168.
- Bernardo KL, McCasland JS, Woolsey TA, Strominger RN (1990) Local intra- and interlaminar connections in mouse barrel cortex. *J Comp Neurol* 291:231–255.
- Borg-Graham LJ, Monier C, Fregnac Y (1998) Visual input evokes transient and strong shunting inhibition in visual cortical neurons. *Nature* 393:369–373.
- Brecht M, Sakmann B (2002a) Whisker maps of neuronal subclasses of the rat ventral posterior medial thalamus, identified by whole-cell voltage recording and morphological reconstruction. *J Physiol (Lond)* 538:495–515.
- Brecht M, Sakmann B (2002b) Dynamic representation of whisker deflection by synaptic potentials in spiny stellate and pyramidal cells in the barrels and septa of layer 4 rat somatosensory cortex. *J Physiol (Lond)* 543:49–70.
- Brumberg JC, Pinto DJ, Simons DJ (1996) Spatial gradients and inhibitory summation in the rat whisker barrel system. *J Neurophysiol* 76:130–140.
- Brumberg JC, Pinto DJ, Simons DJ (1999) Cortical columnar processing in the rat whisker-to-barrel system. *J Neurophysiol* 82:1808–1817.
- Bruno RM, Simons DJ (2002) Feedforward mechanisms of excitatory and inhibitory cortical receptive fields. *J Neurosci* 22:10966–10975.
- Carvell GE, Simons DJ (1988) Membrane potential changes in rat SmI cortical neurons evoked by controlled stimulation of mystacial vibrissae. *Brain Res* 448:186–191.
- Chapin JK (1986) Laminar differences in sizes, shapes, and response profiles of cutaneous receptive fields in the rat SI cortex. *Exp Brain Res* 62:549–559.
- Chung S, Li X, Nelson SB (2002) Short-term depression at thalamocortical synapses contributes to rapid adaptation of cortical sensory responses *in vivo*. *Neuron* 34:437–446.
- Connors BW, Gutnick MJ, Prince DA (1982) Electrophysiological properties of neocortical neurons *in vitro*. *J Neurophysiol* 48:1302–1320.
- Connors BW, Malenka RC, Silva LR (1988) Two inhibitory postsynaptic potentials, and GABA and GABAB receptor-mediated responses in neocortex of rat and cat. *J Physiol (Lond)* 406:443–468.
- Contreras D, Steriade M (1995) Cellular basis of EEG slow rhythms: a study of dynamic corticothalamic relationships. *J Neurosci* 15:604–622.
- Coombs JS, Eccles JC, Fatt P (1955) The inhibitory suppression of reflex discharges from motoneurons. *J Physiol (Lond)* 130:396–413.
- Creutzfeldt OD, Watanabe S, Lux HD (1966) Relations between EEG phenomena and potentials of single cortical cells. I. Evoked responses after thalamic and epicortical stimulation. *Electroencephalogr Clin Neurophysiol* 20:1–18.
- Douglas RJ, Koch C, Mahowald M, Martin KA, Suarez HH (1995) Recurrent excitation in neocortical circuits. *Science* 269:981–985.
- Feldmeyer D, Lubke J, Silver RA, Sakmann B (2002) Synaptic connections between layer 4 spiny neurone-layer 2/3 pyramidal cell pairs in juvenile rat barrel cortex: physiology and anatomy of interlaminar signalling within a cortical column. *J Physiol (Lond)* 538:803–822.
- Goldreich D, Kyriazi HT, Simons DJ (1999) Functional independence of layer IV barrels in rodent somatosensory cortex. *J Neurophysiol* 82:1311–1316.
- Gottlieb JP, Keller A (1997) Intrinsic circuitry and physiological properties of pyramidal neurons in rat barrel cortex. *Exp Brain Res* 115:47–60.
- Hoeflinger BF, Bennett-Clarke CA, Chiaia NL, Killackey HP, Rhoades RW (1995) Patterning of local intracortical projections within the vibrissae

- representation of rat primary somatosensory cortex. *J Comp Neurol* 354:551–563.
- Holt GR, Koch C (1997) Shunting inhibition does not have a divisive effect on firing rates. *Neural Comput* 9:1001–1013.
- Jensen KF, Killackey HP (1987) Terminal arbors of axons projecting to the somatosensory cortex of the adult rat. I. The normal morphology of specific thalamocortical afferents. *J Neurosci* 7:3529–3543.
- Kleinfeld D, Delaney KR (1996) Distributed representation of vibrissa movement in the upper layers of somatosensory cortex revealed with voltage-sensitive dyes. *J Comp Neurol* 375:89–108.
- Kyriazi HT, Simons DJ (1993) Thalamocortical response transformations in simulated whisker barrels. *J Neurosci* 13:1601–1615.
- Land PW, Buffer Jr SA, Yaskosky JD (1995) Barreloids in adult rat thalamus: three-dimensional architecture and relationship to somatosensory cortical barrels. *J Comp Neurol* 355:573–588.
- Llinas R (1964) Mechanisms of supraspinal actions upon spinal cord activities. Differences between reticular and cerebellar inhibitory actions upon alpha extensor motoneurons. *J Neurophysiol* 27:1117–1126.
- Llinas RR (1988) The intrinsic electrophysiological properties of mammalian neurons: insights into central nervous system function. *Science* 242:1654–1664.
- Llinas R, Terzuolo CA (1964) Mechanisms of supraspinal actions upon spinal cord activities. Reticular inhibitory mechanisms on alpha-extensor motoneurons. *J Neurophysiol* 27:579–591.
- Llinas R, Baker R, Precht W (1974) Blockage of inhibition by ammonium acetate action on chloride pump in cat trochlear motoneurons. *J Neurophysiol* 37:522–532.
- McCormick DA, Connors BW, Lighthall JW, Prince DA (1985) Comparative electrophysiology of pyramidal and sparsely spiny stellate neurons of the neocortex. *J Neurophysiol* 54:782–806.
- Moore CI, Nelson SB (1998) Spatio-temporal subthreshold receptive fields in the vibrissa representation of rat primary somatosensory cortex. *J Neurophysiol* 80:2882–2892.
- Moore CI, Nelson SB, Sur M (1999) Dynamics of neuronal processing in rat somatosensory cortex. *Trends Neurosci* 22:513–520.
- Nunez A, Amzica F, Steriade M (1993) Electrophysiology of cat association cortical cells *in vivo*: intrinsic properties and synaptic responses. *J Neurophysiol* 70:418–430.
- Petersen CC, Sakmann B (2001) Functionally independent columns of rat somatosensory barrel cortex revealed with voltage-sensitive dye imaging. *J Neurosci* 21:8435–8446.
- Shimegi S, Ichikawa T, Akasaki T, Sato H (1999) Temporal characteristics of response integration evoked by multiple whisker stimulations in the barrel cortex of rats. *J Neurosci* 19:10164–10175.
- Simons DJ (1978) Response properties of vibrissa units in rat SI somatosensory neocortex. *J Neurophysiol* 41:798–820.
- Simons DJ (1985) Temporal and spatial integration in the rat SI vibrissa cortex. *J Neurophysiol* 54:615–635.
- Simons DJ, Carvell GE (1989) Thalamocortical response transformation in the rat vibrissa/barrel system. *J Neurophysiol* 61:311–330.
- Swadlow HA (2003) Fast-spike interneurons and feedforward inhibition in awake sensory neocortex. *Cereb Cortex* 13:25–32.
- Swadlow HA, Gusev AG, Bezdudnaya T (2002) Activation of a cortical column by a thalamocortical impulse. *J Neurosci* 22:7766–7773.
- Tamas G, Buhl EH, Somogyi P (1997) Fast IPSPs elicited via multiple synaptic release sites by different types of GABAergic neuron in the cat visual cortex. *J Physiol (Lond)* 500:715–738.
- Thomson AM, West DC, Wang Y, Bannister AP (2002) Synaptic connections and small circuits involving excitatory and inhibitory neurons in layers 2–5 of adult rat and cat neocortex: triple intracellular recordings and biocytin labelling *in vitro*. *Cereb Cortex* 12:936–953.
- Welker C (1976) Receptive fields of barrels in the somatosensory neocortex of the rat. *J Comp Neurol* 166:173–189.
- Welker C, Woolsey TA (1974) Structure of layer IV in the somatosensory neocortex of the rat: description and comparison with the mouse. *J Comp Neurol* 158:437–453.
- Woolsey TA, Van der Loos H (1970) The structural organization of layer IV in the somatosensory region (SI) of mouse cerebral cortex. The description of a cortical field composed of discrete cytoarchitectonic units. *Brain Res* 17:205–242.
- Zhu JJ, Connors BW (1999) Intrinsic firing patterns and whisker-evoked synaptic responses of neurons in the rat barrel cortex. *J Neurophysiol* 81:1171–1183.